Available online at www.sciencedirect.com
ScienceDirect
Trans. Nonferrous Met. Soc. China 35(2025) 2846−2858
Transactions of Nonferrous Metals Society of China
www.tnmsc.cn

Effect of rapid cold stamping on microstructure and mechanical properties of spray-formed Al−Zn−Mg−Cu alloy

Cai-he FAN, Ji LI, Shuang-jun YANG, Ze-yi HU, Qin WU, Ling OU, Shuai WU

College of Materials Science and Engineering, Hunan University of Technology, Zhuzhou 412007, China

Received 18 February 2024; accepted 5 March 2025

Abstract: X-ray diffraction (XRD), scanning electron microscopy (SEM), energy-dispersive spectroscopy (EDS), electron backscatter diffraction (EBSD), and transmission electron microscopy (TEM) were used to systematically investigate the impact of rapid cold stamping on microstructural evolution and mechanical properties of spray-formed Al−Zn−Mg−Cu alloys under ambient conditions. The results reveal that the dislocation density increases with successive cold stamping passes, the volume fraction of the secondary phase ($Mg(Zn,Cu,Al)_2$) increases from 15.64% to 23.94%, and the average size decreases from 1.41 to 0.75 μm. The pinning effect of the secondary phases on dislocations promotes a significant transformation from low-angle grain boundaries to high-angle grain boundaries, resulting in the average grain size decreasing from 5.75 to 0.97 μm. The strength and hardness of the samples increase with successive cold stamping passes, which is attributed to the synergistic effects of dislocation strengthening, grain boundary strengthening, and secondary phase strengthening.

Key words: Al−Zn−Mg−Cu alloy; rapid cold stamping; texture; sub-grain boundaries; secondary phase

1 Introduction

The Al−Zn−Mg−Cu alloy, known for its low density, high specific strength, superior plasticity, and outstanding corrosion resistance, has emerged as a key structural material in the aerospace sector [1−3]. Severe plastic deformation (SPD) is recognized as a highly effective technique for enhancing the microstructure and mechanical properties of this alloy, attracting considerable global research interest [4,5]. CHUNG et al [6] investigated the Al−Zn−Mg−Cu alloy via upsetting-extrusion (UE), demonstrating that this method notably reduces the size disparity between fine and coarse grains in the bimodal structure of the alloy, while also inducing a pronounced copper/ cubic texture. DUCHAUSSOY et al [7] observed that the Al_7Cu_2Fe intermetallic particles in the alloy fractured after 10 passes of high-pressure torsion at ambient temperature. HIDALGO-MANRIQUE et al [8] applied accumulative roll-bonding to 7075 aluminum alloy and found that increasing the rolling strain or number of passes substantially reduced the average grain size from 457 to 363 nm. YANG et al [9] investigated the effects of varying degrees of hot rolling deformation on the Al−Zn−Mg−Cu alloy. Their results revealed that as deformation increased, LAGBs transformed into HAGBs, and equiaxed grains with low dislocation density evolved into fibrous structures with high dislocation density. ZHAO et al [10] studied the influence of multidirectional forging effects on the microstructural evolution of a high-density precipitate Al−Zn−Mg−Cu alloy. Their results demonstrated that dislocations were effectively pinned by precipitates during deformation, leading to substantial grain refinement at temperatures of 300 and 350 °C.

Corresponding author: Cai-he FAN, Tel: +86-731-22183466, E-mail: 369581813@qq.com
https://doi.org/10.1016/S1003-6326(25)66852-X

Rapid cold stamping, a severe plastic deformation technique, is gaining recognition for its advantages, including low deformation temperature (25 °C), substantial strain, and high strain rate. ZHANG et al [11] investigated the relationship between microstructure and high-impact resistance in Al−0.7Sc alloy under high-speed impacts. ZHOU et al [12] examined the role of precipitated phases in the dynamic impact toughness of Al−Cu alloys, revealing that the nano θ'' and θ' phases notably enhance impact toughness by strengthening the α-Al matrix. LU et al [13] simulated the hot stamping process for the Al−Zn−Mg−Cu alloy at elevated temperatures to examine its effects on microstructural evolution and mechanical properties.

Previous studies [14] studied the impact of rapid cold stamping on the microstructural evolution of spray-formed Al−Cu−Mg alloys. A pronounced reduction in grain and precipitate sizes was observed with an increasing number of deformation passes, accompanied by substantial enhancement in dislocation density and mechanical properties. However, research on the effects of rapid cold stamping on the microstructure of spray-formed Al−Zn−Mg−Cu alloys is limited. Building on this foundation, the present study investigated the influence of rapid cold stamping on the microstructure of spray-formed Al−Zn−Mg−Cu alloys at ambient temperatures. This study explored the evolution of the secondary phase, grain and grain boundaries, dislocation density, and texture. Moreover, the study elucidated the mechanisms underlying grain refinement and the increase in hardness under rapid cold stamping conditions, providing a theoretical basis for enhancing the comprehensive performance of spray-formed Al−Zn−Mg−Cu alloys.

2 Experimental

The spray-formed rapidly solidified Al−Zn−Mg−Cu alloy cylindrical billet was prepared using a self-developed SD380 large-scale spray forming equipment. The chemical composition of the alloy is presented by a FOUNDRY-MASTER Smart direct reading spectrometer, as shown in Table 1. The cylindrical billet was initially extruded into a *d*23 mm round bar on a 1250 t extrusion press. The extrusion was performed at a temperature of 450 °C with an extrusion ratio of 15∶1. Subsequently, the round bar was cut into cylinders with dimensions of *d*23 mm × 42 mm using a wire cutting machine. These cylinders were then annealed in a muffle furnace at 450 °C for 0.5 h and allowed to cool inside the furnace. Finally, the cylinders were placed in a custom-designed stamping mold and subjected to three cycles of rapid cold stamping to fabricate aluminum alloy cartridges. After each stamping pass, the cylinders were returned to the muffle furnace for additional annealing. A schematic of the rapid cold stamping process is shown in Fig. 1.

Table 1 Composition of alloy (wt.%)

Zn	Mg	Cu	Zr	Fe	Al
6.54	1.96	2.53	0.113	<0.1	Bal.

Samples were selected from the wall of the cylinder formed through extrusion, annealing, and rapid cold stamping for microstructural observation and hardness testing. The microstructure and dislocation distribution of these samples were analyzed using a FEI Tecnai F30 transmission electron microscope (TEM). TEM samples were prepared using a Fischione 1051 ion milling machine, employing a multistage ion beam energy and milling angle adjustment method. In the first stage, the ion beam energy was set to be 5 kV with a milling angle of 8°, and the milling time was 60 min. In the second stage, the ion beam energy was reduced to 4 kV, the milling angle was adjusted to be 7°, and the milling time was set to be 10 min. The final stage involved an ion beam energy of 2.5 kV, a milling angle of 6°, and a duration of 30 min. A liquid nitrogen cooling stage was utilized throughout the preparation process to minimize thermal damage to the sample. A vacuum transfer device was then used to isolate the sample from water and oxygen exposure.

Phase analysis of the samples was performed using a D/max2500 18 kW rotating target X-ray diffractometer, with a scanning speed of 10 (°)/min. The size and volume fraction of the secondary phase were observed using a SEM−5000. The grain morphology, texture, grain boundaries, and kernel average misorientation (KAM) were characterized by an electron backscatter diffraction (EBSD) probe. The observed samples were taken perpendicular to the extrusion and cold forging directions. The

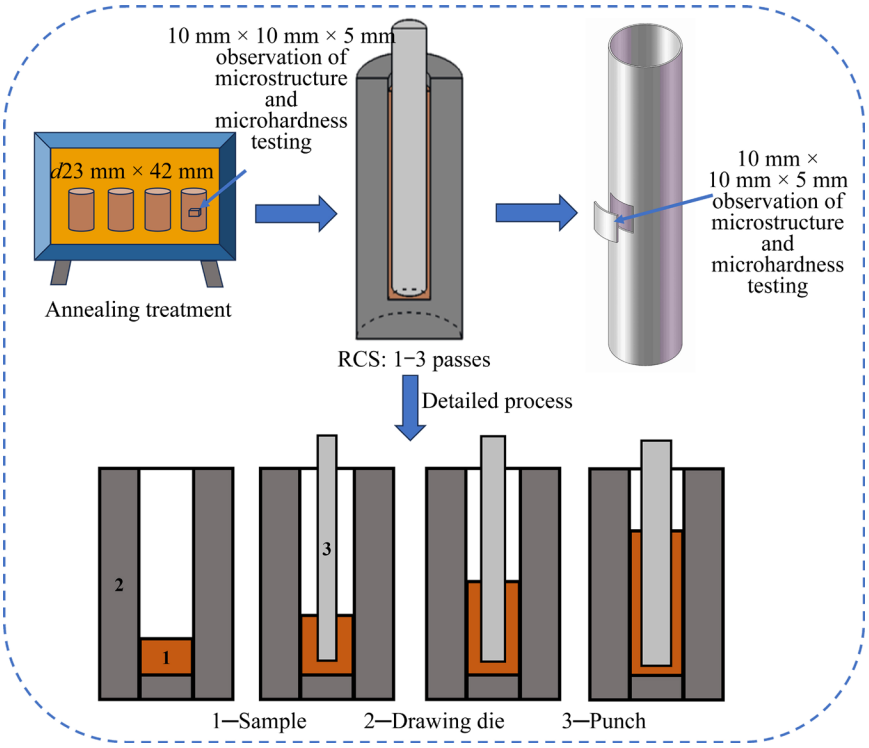

Fig. 1 Schematic diagram of rapid cold stamping sample

hardness of the samples was measured using a Leica Vickers hardness tester, with a load of 500 g applied for 5 s, and the average value was taken from 10 measurements per sample. Tensile properties were evaluated using an Instron 3369 universal testing machine at a tensile rate of 2 mm/min. Three replicates were prepared for each sample, and the average value was used as the final test result.

3 Results

3.1 Microstructural evolution

3.1.1 Secondary phases

The X-ray diffraction (XRD) patterns of the Al−Zn−Mg−Cu alloy in its extruded, annealed, and various rapid cold stamping states are shown in Fig. 2. The patterns reveal diffraction peaks corresponding to the aluminum matrix, along with faint peaks attributed to the $MgZn_2$ phase in the extruded samples. After annealing, the diffraction peak of the aluminum matrix is further intensified, while the peak for the $MgZn_2$ phase shows minimal change. Following rapid cold stamping, the diffraction peak for the $MgZn_2$ phase becomes more prominent, with its relative intensity increasing as the number of stamping passes rises. The enhanced diffraction peaks of the $MgZn_2$ phase in samples

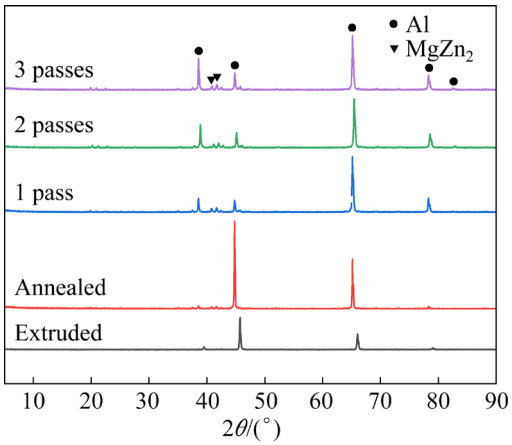

Fig. 2 XRD patterns of Al−Zn−Mg−Cu alloy before and after rapid cold stamping deformation

subjected to multiple cold stamping passes indicate dynamic precipitation during the SPD process, which is consistent with the findings of SHEN et al [15].

Figure 3 shows the evolution of the secondary phases in the alloy after extrusion, annealing, and various rapid cold stamping deformations. As shown in Fig. 3(a), the extruded alloy contains large secondary-phase particles (1.5 μm) as well as smaller ones (0.2 μm). Figures 3(c−e) show that the secondary-phase particles become fragmented and refined, achieving a more uniform distribution. The

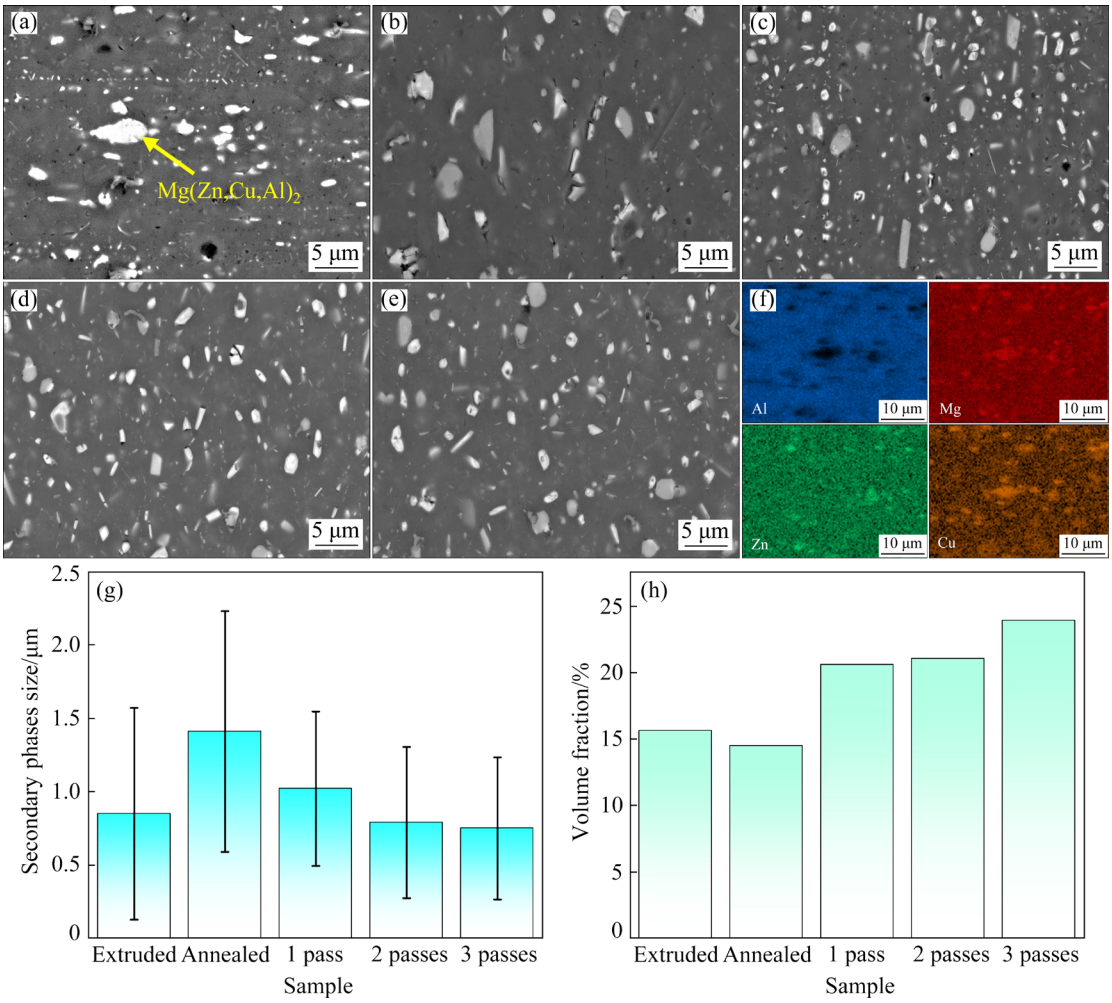

Fig. 3 SEM images of Al−Zn−Mg−Cu alloy after rapid cold stamping in different states and passes: (a) Extruded; (b) Annealed; (c) 1 pass; (d) 2 passes; (e) 3 passes; (f) EDS results corresponding to (a); (g) Statistical diagram of secondary phase size; (h) Statistical diagram of volume fraction

energy dispersive spectroscopy (EDS) results presented in Fig. 3(f) indicate that the large secondary-phase particles are identified as the $Mg(Zn,Cu,Al)_2$ phase, which is consistent with the XRD results and the findings of LI et al [16]. Figure 3(g) quantifies the secondary-phase particle sizes under various conditions, recording sizes of 0.85, 1.41, 1.02, 0.79, and 0.75 μm, while Fig. 3(h) shows the secondary-phase volume fractions of the alloy at 15.64%, 14.49%, 20.61%, 21.06%, and 23.94%, respectively. The results show that the reduction in average size of the secondary phase and the increase in volume fraction with the rise of cold stamping passes can be attributed to the increasing degree of plastic deformation.

3.1.2 Grains

The EBSD maps of the alloy after extrusion and annealing are shown in Fig. 4, where the scan step size is 0.4. As shown in Fig. 4, the grains are predominantly elongated, with a few equiaxed grains observed in the extruded and annealed states. The average grain size of the alloy increases from 5.41 to 5.75 μm after annealing.

Figure 5 illustrates the EBSD images of the Al−Zn−Mg−Cu alloy after multiple passes of rapid cold stamping deformation, with a scan step size of 0.09 μm. Figures 5(a, c, e) show different color contrasts, which correspond to distinct grain orientations. In Fig. 5(a), notable alterations in grain morphology and size are observed after 1 pass of rapid cold stamping. The elongated grains from the extruded and annealed states transform into equiaxed grains, with a prominent orientation along ⟨001⟩ and ⟨111⟩. As illustrated in Figs. 5(c) and (e), the grains are refined after the second and third passes of rapid cold stamping, respectively, and the grain orientations are also changed. Figures 5(b, d, f) illustrate the reduction in average

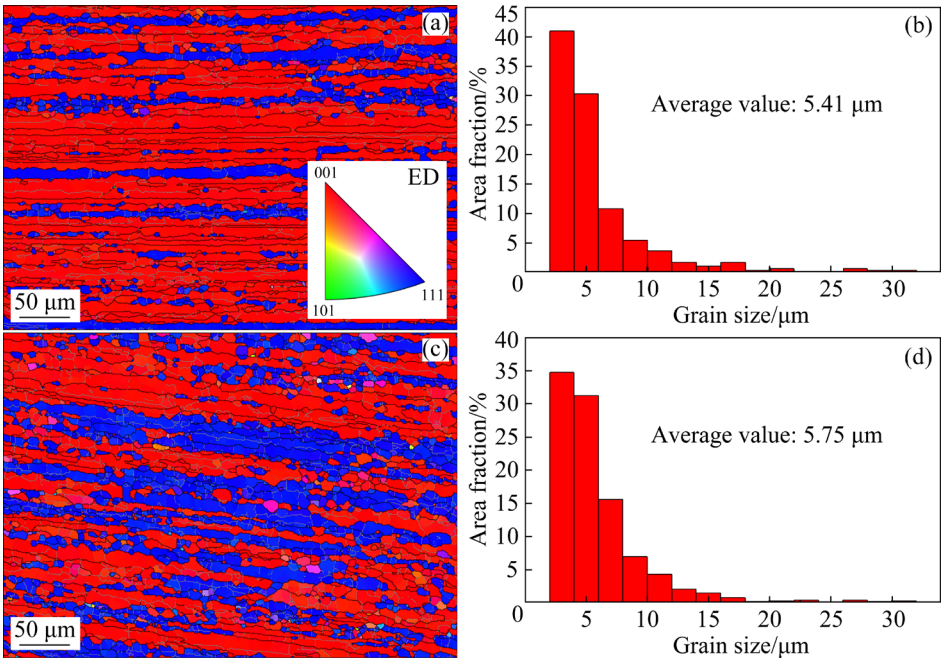

Fig. 4 EBSD images (a, c), and grain size distribution diagrams (b, d) of Al−Zn−Mg−Cu alloy after extrusion (a, b) and annealing (c, d)

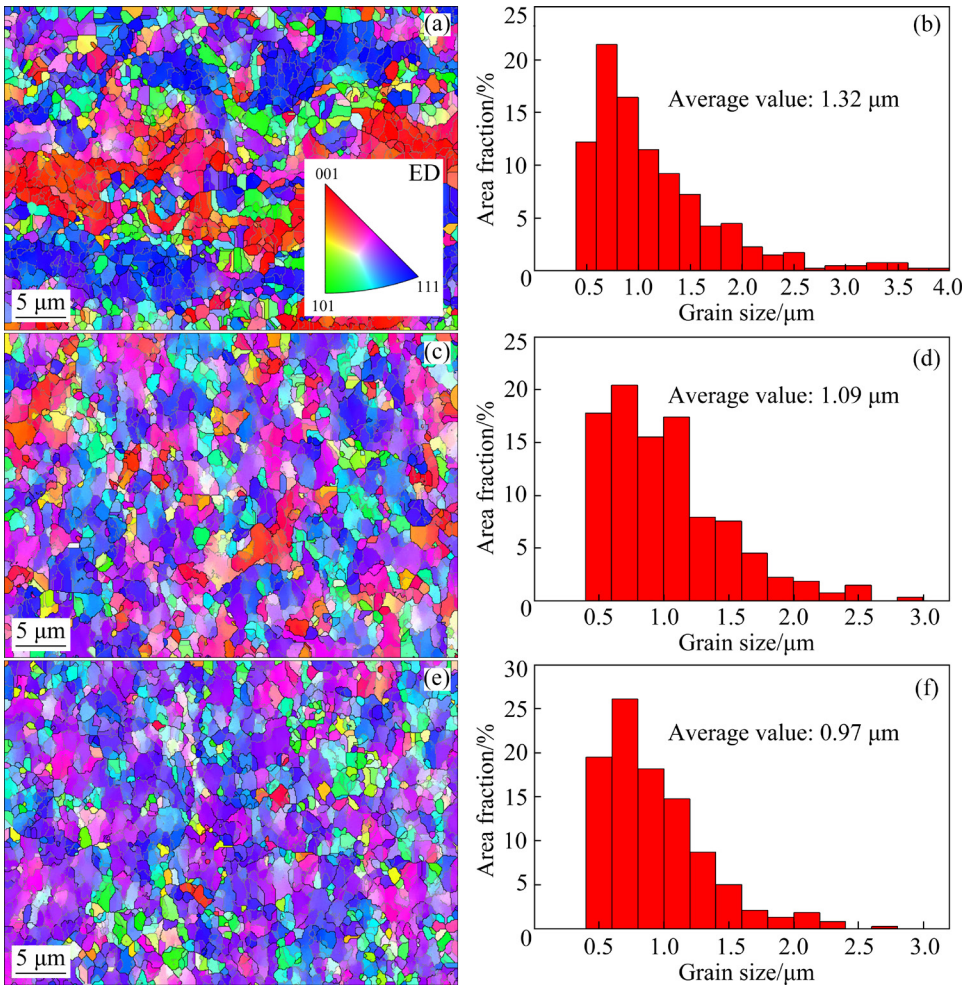

Fig. 5 EBSD images (a, c, e), and grain size distribution diagrams (b, d, f) of Al−Zn−Mg−Cu alloy after rapid cold stamping: (a, b) 1 pass; (c, d) 2 passes; (e, f) 3 passes

grain size across various stamping passes, with the grain size decreasing from 1.32 to 0.97 μm. This reduction highlights the correlation between the number of cold stamping passes and the progressive refinement of the alloy's grain size.

3.1.3 Grain boundary and dislocations

Figure 6 shows the grain boundary distribution of the Al−Zn−Mg−Cu alloy after varying passes of rapid cold stamping deformation. Back lines indicate LAGBs, whereas green lines indicate HAGBs. In Fig. 6(a), LAGBs comprise the majority of the grain boundaries, accounting for 74.5% of the alloy after 1 pass of cold stamping, while HAGBs constitute only 25.5%. In Fig. 6(b), after 2 passes of cold stamping, LAGBs account for 69.2% of the grain boundaries, while HAGBs increase to 30.8%. In Fig. 6(c), HAGBs further increase to 44.2% after 3 passes of cold stamping.

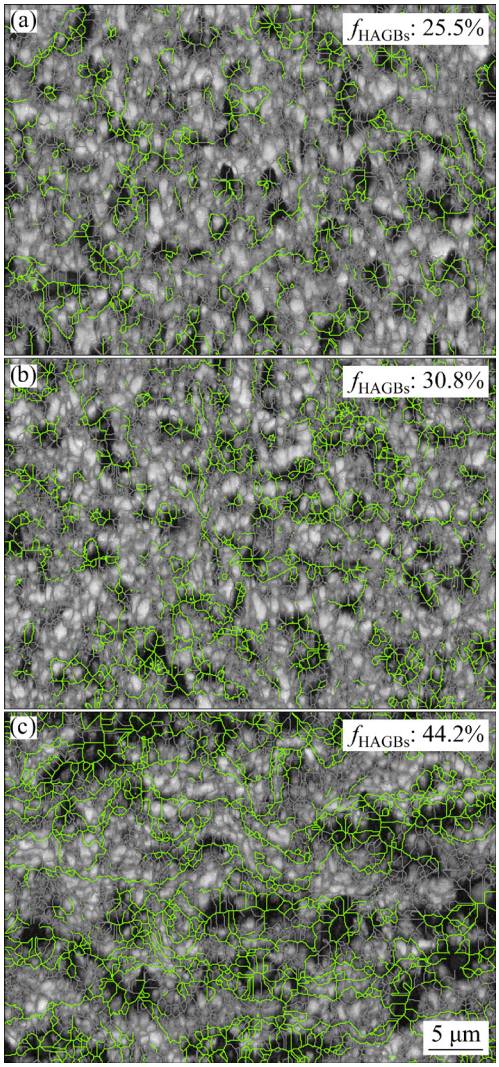

Fig. 6 Grain boundary distribution of Al−Zn−Mg−Cu alloy after rapid cold stamping: (a) 1 pass; (b) 2 passes; (c) 3 passes

In the field of materials science, understanding the correlation between deformation and dislocation density is crucial for explaining material behavior under stress. The KAM quantifies the average misorientation between a given point and its neighboring points, serving as an effective measure of the extent of deformation within a grain [17]. Figure 7 presents the KAM maps and distribution histograms of the Al−Zn−Mg−Cu alloy after rapid cold stamping. As depicted in Fig. 7(a), a KAM value of 0.41° after extrusion indicates a relatively low dislocation density. After annealing, Fig. 7(b) shows a further decrease in dislocation density to 0.35°. Figures 7(c−e) display KAM maps for the samples subjected to rapid cold stamping, illustrating an increase in green areas at coarse grain boundaries and within the grains, while fine grains predominantly exhibit blue interiors. This color distribution indicates a heightened concentration of dislocations at grain boundaries and within large grains [9]. After 1 pass of rapid cold stamping, the average KAM value rises to 0.48°, and after 3 passes, the average KAM further increases to 0.58°.

Figures 6 and 7 demonstrate that substantial dislocation formation occurs during the rapid cold stamping process, leading to the development of dislocation tangles within specific regions of the grains. These tangles facilitate the formation of numerous LAGBs. Additionally, as the number of cold stamping passes increases, some LAGBs gradually transform into HAGBs, contributing to the formation of ultrafine grains.

Figures 8(a−c) show the TEM images of the Al−Zn−Mg−Cu alloy after multiple rapid cold stamping passes. These images clearly illustrate that dislocation density increases within the alloy as the number of rapid cold stamping passes increases. Figure 8(d) reveals the selected area electron diffraction pattern corresponding to Fig. 8(a), captured with the electron beam being directed along the ⟨110⟩ crystallographic direction of the matrix. This pattern displays two distinct types of diffraction spots, identified as the η' phase and Al_3Zr. Dislocations typically experience a dynamic process of accumulation and annihilation during deformation [18], as illustrated in Fig. 8(c). Precipitates effectively pin the movement of dislocations and hinder the migration of sub-grain boundaries. In alloys such as aluminum, which has high stacking fault energy, dislocations generated

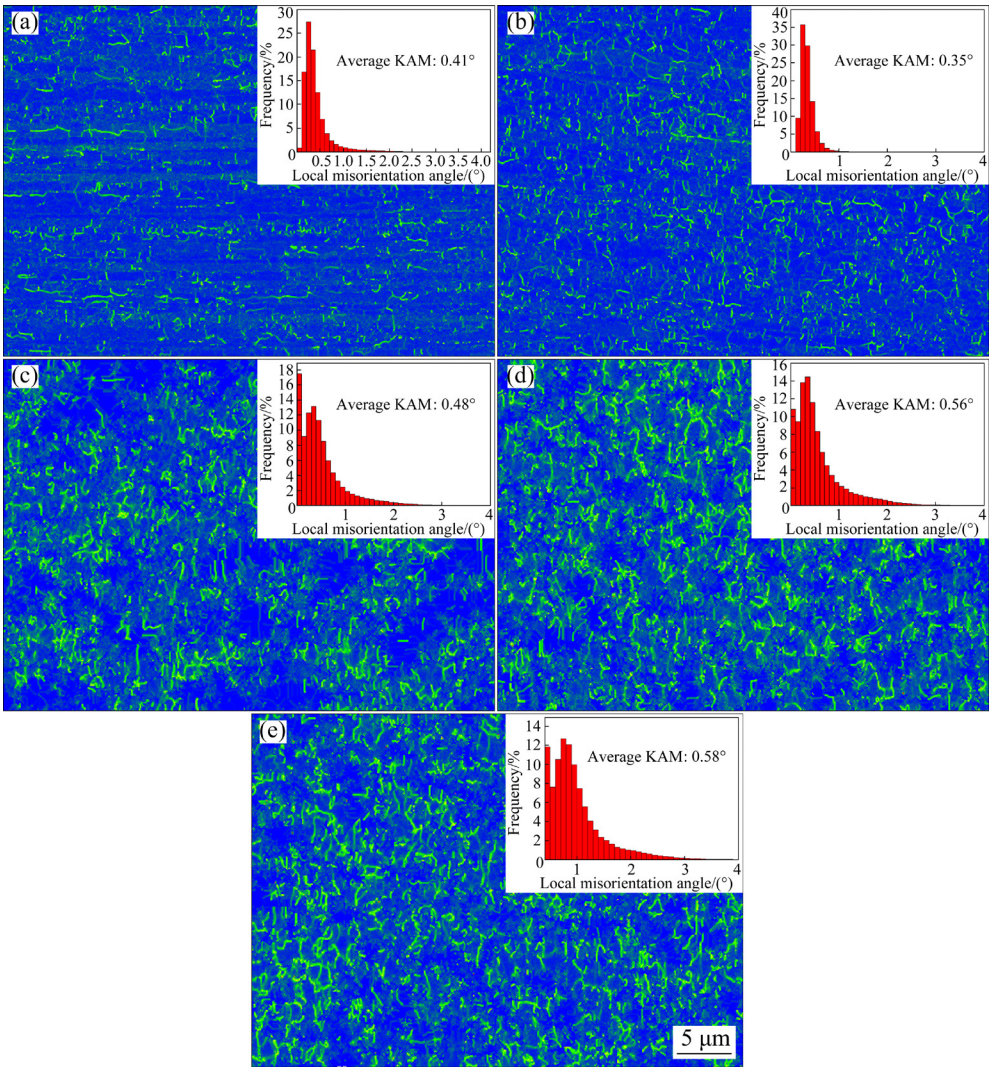

Fig. 7 KAM maps and distribution histograms of Al−Zn−Mg−Cu alloy after rapid cold stamping: (a) Extruded; (b) Annealed; (c) 1 pass; (d) 2 passes; (e) 3 passes

during thermal deformation are progressively absorbed by sub-grain boundaries [19]. Thus, LAGBs are converted into HAGBs, leading to the formation of fine grains. During the deformation of the Al−Zn−Mg−Cu alloy, numerous LAGBs and several isolated HAGBs emerge within the deformed grains, consistent with the findings presented in Fig. 6, which have been proven by many researchers through EBSD [20,21,22]. As LAGBs absorb an increasing numbers of dislocations and transition into HAGBs with additional deformation passes, the proportion of LAGBs gradually decreases, whereas that of HAGBs correspondingly rises. This transition is primarily attributed to the role of precipitates in hindering the migration of sub-grain boundaries, which facilitates the conversion of LAGBs to HAGBs, as depicted in Fig. 8(c).

3.2 Mechanical properties

Figure 9 shows the variations in mechanical properties of the Al−Zn−Mg−Cu alloy under different conditions and subsequent to various cold stamping passes, with corresponding values listed in Table 2. The ultimate tensile strength (UTS) of the extruded alloy is measured at 379.2 MPa, accompanied by an elongation (EL) of 15.21% and a hardness of HV 130.33. After annealing, the UTS and hardness decrease to 305.6 MPa and HV 78.74, respectively, while the elongation increases to 23.47%. Further cold stamping passes lead to notable improvement in the alloy's strength and hardness. After 3 passes of rapid cold stamping, the UTS and hardness increase to 518.3 MPa and HV 124.96,

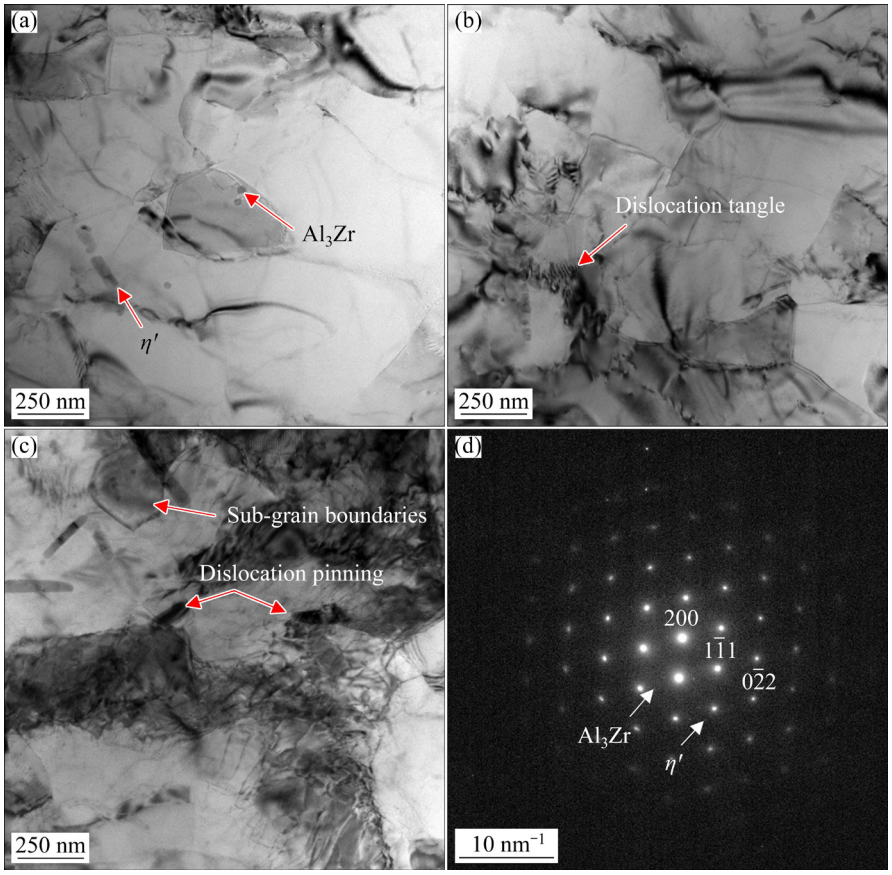

Fig. 8 TEM images of rapid cold stamping samples with different passes: (a) 1 pass; (b) 2 passes; (c) 3 passes; (d) Selected area electron diffraction pattern along ⟨110⟩ crystal band axis of matrix corresponding to (a)

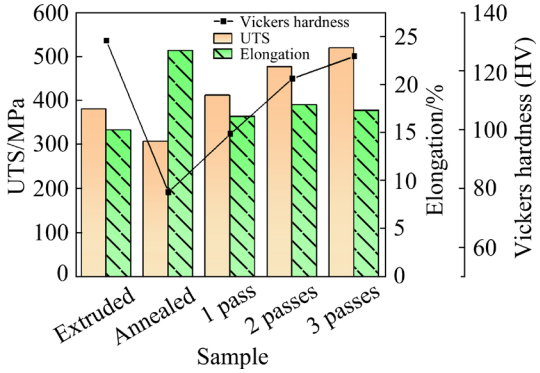

Fig. 9 Changes in mechanical properties of Al−Zn−Mg−Cu alloy after rapid cold stamping in different states and passes

respectively, showing improvements of 70% and 114%, respectively, compared with the annealed condition. The EL following 1 to 3 passes of rapid cold stamping were 16.62%, 17.83%, and 17.25%, respectively, with minimal changes observed in the EL. The enhancement in alloy strength after deformation is mainly attributed to grain refinement, elevated dislocation density, and impeding effects of precipitated phases.

Table 2 Mechanical properties of Al−Zn−Mg−Cu alloy after rapid cold stamping in different states and passes

Sample	UTS/MPa	EL/%	Vickers hardness (HV)
Extruded	379.2	15.21	130.33
Annealed	305.6	23.47	78.74
1 pass	410.7	16.62	98.55
2 passes	475.3	17.83	117.43
3 passes	518.3	17.25	124.96

4 Discussion

4.1 Effect of rapid cold stamping on grain refinement

Detailed analyses utilizing XRD, SEM, EBSD, and TEM have elucidated the mechanisms underlying grain refinement in the Al−Zn−Mg−Cu alloy during rapid cold stamping deformation. After extrusion, the alloy exhibits a refined grain size and a notable increase in dislocation density [23]. Following successive passes of rapid cold stamping deformation, the dislocation density in the extruded

alloy intensifies, precipitating the formation of numerous LAGBs. The high-density dislocations reorganize with an increasing number of cold stamping passes, and some LAGBs evolve into HAGBs, further enhancing grain refinement [24−27]. WANG et al [28] successfully obtained high-strength, ultrafine-grained pure aluminum through extensive-pass isothermal extrusion and cold rolling.

As previously discussed, grain refinement is primarily conducted through the dislocation rearrangement and the transformation of LAGBs, with the specific mechanisms depicted in Fig. 10. With an increasing number of deformation passes, high-density dislocations begin to accumulate within the grains. Numerous dislocations lead to the formation of dislocation stacking and entanglement at grain boundaries and within the secondary phases, facilitating the formation of areas with high dislocation density. Subsequently, these unordered dislocations progressively transform into ordered dislocation walls as deformation energy storage increases alongside high dislocation density, eventually rearranging into LAGBs. Ultimately, certain sub-grain boundaries and LAGBs will evolve into HAGBs, culminating in the formation of new fine grains.

4.2 Effect of rapid cold stamping on texture evolution

EBSD data were employed to analyze the texture of the Al−Zn−Mg−Cu alloy in diverse states to elucidate the evolution of textures under varying deformation conditions. Figure 11 displays the orientation distribution function (ODF) sections of the alloy under different thermal deformation conditions. Figure 11(a) shows that the grain orientation of the extruded alloy predominantly aligns with the angles (0°, 0°−90°, and 90°). The Miller index confirms that the extrusion direction is parallel to the ⟨100⟩ direction, indicating the presence of a ⟨100⟩ filamentary texture in the extruded specimen. As shown in Fig. 11(b), the annealed specimen exhibits a notable peak density near the Goss orientation (0°, 45° and 90°), with corresponding Miller indexes of {110}⟨100⟩, indicating a sustained predominance of the ⟨100⟩ filamentary texture. Additionally, the annealed specimens demonstrate an increased density of random orientations. Figure 11(d) reveals that following the second pass of cold stamping, the orientation of the sample primarily centers around 70°, 0°−45°, and 90°, with a predominant distribution near ⟨130⟩, ⟨113⟩, and ⟨122⟩, respectively. Figure 11(e) indicates that after 3 passes of cold

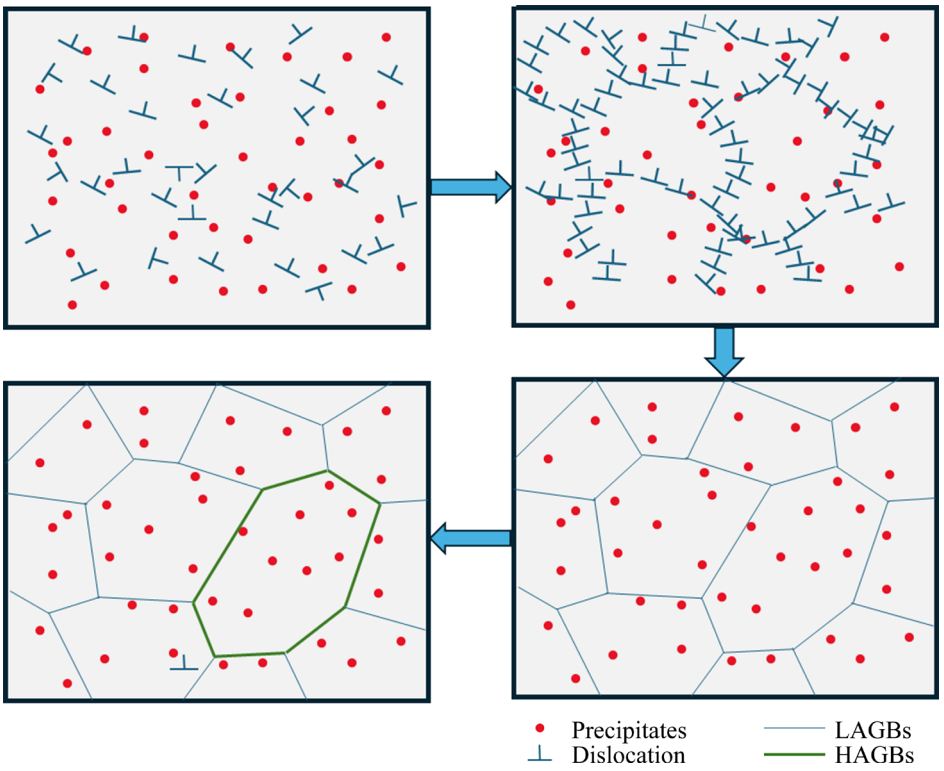

Fig. 10 Mechanism of rapid cold stamping for grain refinement

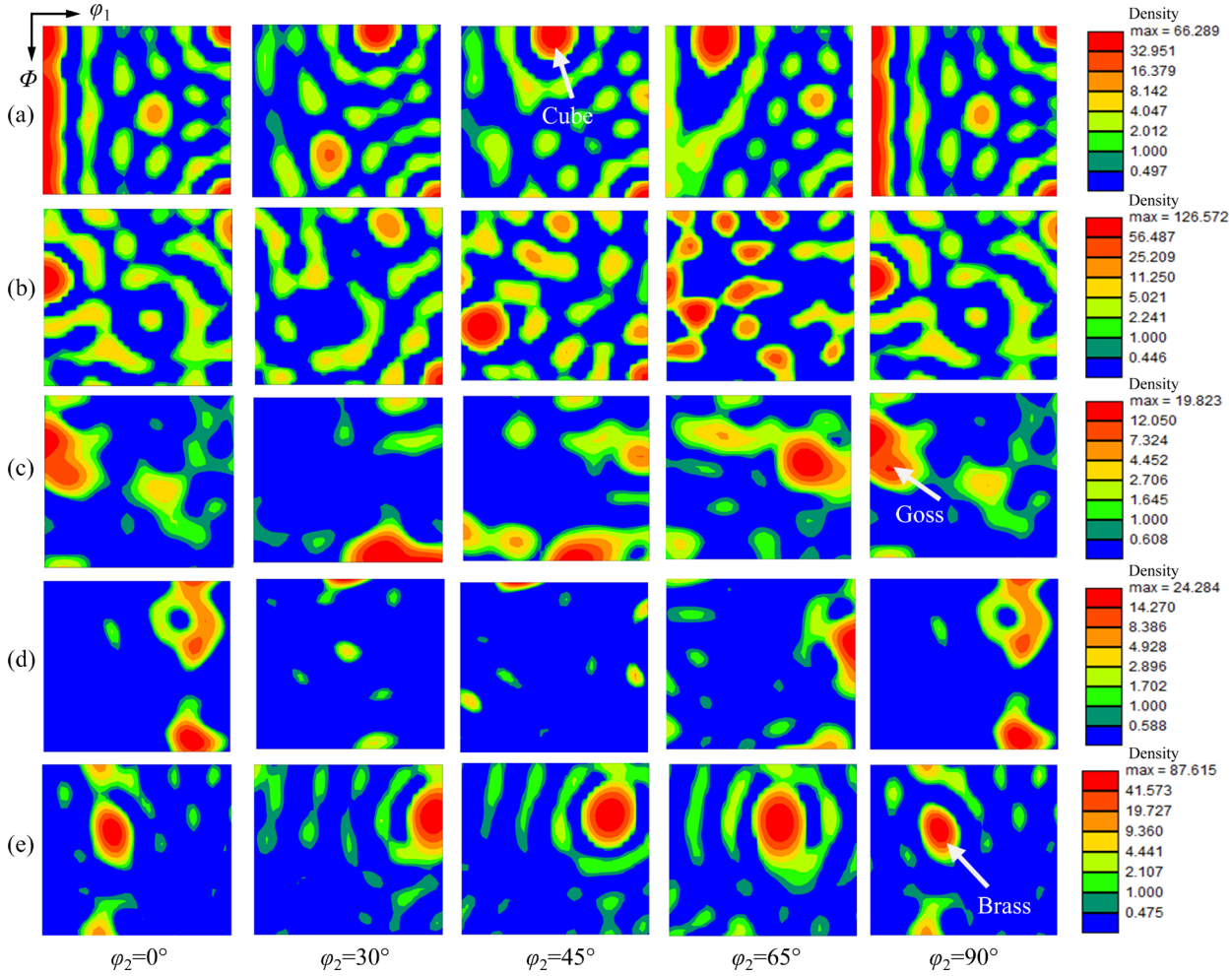

Fig. 11 ODF cross-section under different conditions: (a) Extruded; (b) Annealed; (c) 1 pass; (d) 2 passes; (e) 3 passes

stamping, the orientation of the sample is mainly concentrated around Brass orientations (35°, 45° and 90°), (90°, 45° and 30°), and (75°, 45° and 45°), with corresponding Miller indexes of {011}⟨121⟩, {001}⟨122⟩, and {230}⟨122⟩, respectively. This finding indicates that the dominant filamentary textures of the sample are ⟨122⟩ and ⟨112⟩. The aforementioned texture types are identified in the standard reverse pole figure, as illustrated in Fig. 12. Notably, with successive cold stamping passes, the principal orientation of the sample transitions from ⟨100⟩ toward ⟨130⟩ and ⟨113⟩, and subsequently toward ⟨112⟩ and ⟨122⟩. This finding implies a rotation of the extrusion direction's orientation from ⟨100⟩ toward orientations closer to ⟨111⟩. Several studies [29,30] indicate that the ⟨111⟩ orientation represents a stable configuration for extruded aluminum alloys, implying that the orientation of the sample stabilizes as the number of cold stamping passes increases.

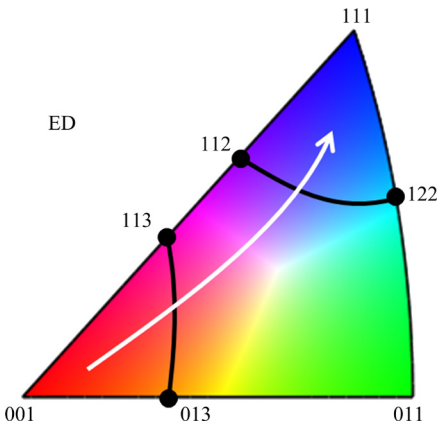

Fig. 12 Evolution of texture in inverse diagram

4.3 Strengthening mechanism

During rapid cold stamping deformation, the main strengthening mechanisms of Al−Zn−Mg−Cu alloy are secondary-phase strengthening (σ_p), dislocation strengthening (σ_d), and fine grain strengthening (σ_g). The corresponding yield strength (YS, σ_y) can be calculated by the following equation [31,32]:

$$\sigma_y=\sigma_o+\sigma_p+\sigma_d+\sigma_g \quad (1)$$

where σ_o is the YS of the pure Al (σ_o=35 MPa) [31]. A substantial alteration in the dislocation density of the alloy is observed during plastic deformation. The contribution of the dislocation strengthening mechanism to the alloy strength can be quantitatively assessed using the Bailey−Hirsch relationship [33]:

$$\sigma_d=M\alpha Gb\rho^{1/2} \quad (2)$$

where M, α, G, b and ρ are the mean orientation factor (M=3.06), a constant (α=0.2), shear modulus (G=27 GPa), amplitude of Burgers vector (b=0.286) and dislocation density of the alloy, respectively. The equation to calculate the density of geometrically necessary dislocations (GND, ρ_{GND}) in the alloy is [34]

$$\rho_{GND}=2KAM_{ave}/(\mu b) \quad (3)$$

where KAM_{ave} is the average of the kernel mean error orientation of the sample, and μ is the scan step size (μ=0.09 μm). The KAM average value is used to represent the density of GND. The analysis reveals that with increasing rapid cold stamping passes, the average GND density substantially escalates from 3.7×10^{16} to 4.5×10^{16} m^{-2}. According to Eqs. (2) and (3), the strength of the alloy increases with dislocation density. Therefore, the dislocation density increases with the rise of cold stamping passes, and the microhardness of the deformed alloy increases. For the fine grain strengthening mechanism, the Hall–Petch relationship can be used [31,35,36,37].

$$\sigma_g=kd^{-1/2} \quad (4)$$

where d and k are the average grain size and material-related parameter (k=0.12 MPa·$m^{1/2}$), respectively [33]. Calculating the reinforcement due to the secondary phase is complicated, and an estimation can be performed using the subsequent equation:

$$\sigma_p=\sigma_y-(\sigma_o+\sigma_d+\sigma_g) \quad (5)$$

Utilizing Eqs. (1)−(5), the contributions of σ_p, σ_d, and σ_g to the strength of the aluminum alloy are quantified, as detailed in Table 3. As indicated in Table 3, the synergistic effects of secondary-phase strengthening, dislocation strengthening, and fine grain strengthening jointly enhance the strength of the alloy.

Table 3 Contribution of strengthening mechanism to Al−Zn−Mg−Cu alloy under different rapid cold stamping passes

Sample	σ_o/ MPa	σ_p/ MPa	σ_d/ MPa	σ_g/ MPa	YS/ MPa
1 pass	35	104.6	91.1	118.8	349.5
2 passes	35	130.1	97.8	135.2	398.1
3 passes	35	152.3	100.6	138.9	426.8

5 Conclusions

(1) Throughout the rapid cold stamping process, severe plastic deformation leads to the fragmentation and refinement of the secondary phase ($Mg(Zn,Cu,Al)_2$), reducing its size from 1.41 to 0.75 μm and enhancing its uniformity.

(2) With successive rapid cold stamping passes, the dislocation density in the alloy markedly increases. Owing to the pinning effect of precipitates on the dislocations, the grain size is substantially refined, with the average grain size diminishing from 5.75 to 0.97 μm.

(3) The enhancement of strength and microhardness is primarily attributed to dislocation strengthening, complemented by synergistic effects from fine-grained and secondary-phase strengthening.

CRediT authorship contribution statement

Cai-he FAN: Formal analysis, Methodology, Conceptualization, Software, Resource; **Ji LI:** Writing − Original draft, Visualization, Investigation; **Shuang-jun YANG** and **Ze-yi HU:** Writing − Review & editing, Conceptualization; **Qin WU** and **Ling OU:** Writing − Review & editing, English correction; **Shuai WU**：Data curation.

Declaration of competing interest

The authors declare that they have no known competing financial interests or personal relationships that could have appeared to influence the work reported in this paper.

Acknowledgments

This work was supported by the National Natural Science Foundation of China (No. 52271177).

References

[1] de SALVO JOÃO G J, AFONSO CONRADO R M. Fatigue strength and microstructure evaluation of Al 7050 alloy wires recycled by spray forming, extrusion and rotary swaging [J].

Transactions of Nonferrous Metals Society of China, 2020, 30(12): 3195−3209.

[2] YUAN Ding-ling, CHEN Song-yi, CHEN Kang-hua, HUANG Lan-ping, CHANG Jiang-yu, ZHOU Liang, DING Yun-feng. Correlations among stress corrosion cracking, grain-boundary microchemistry, and Zn content in high Zn-containing Al−Zn−Mg−Cu alloys [J]. Transactions of Nonferrous Metals Society of China, 2021, 31(8): 2220−2231.

[3] CASSELL A M, ROBSON J D, RACE C P, EGGEMAN A, HASHIMOTO T, BESEL M. Dispersoid composition in zirconium containing Al−Zn−Mg−Cu (AA7010) aluminium alloy [J]. Acta Materialia, 2019, 169: 135−146.

[4] SAFYARI M, HOJO T, MOSHTAGHI M. Effect of environmental relative humidity on hydrogen-induced mechanical degradation in an Al−Zn−Mg−Cu alloy [J]. Vacuum, 2021, 192: 110489.

[5] WANG Fei-fan, MENG Wen, ZHANG Hong-wei, HAN Zhi-qiang. Effects of under-aging treatment on micro-structure and mechanical properties of squeeze-cast Al−Zn−Mg−Cu alloy [J]. Transactions of Nonferrous Metals Society of China, 2018, 28(10): 1920−1927.

[6] CHUNG T F, YEH C W, LIAW Y S, LIN J R, HO P L, HSIAO C N, TSAO C S, CHOU C M, YANG Y L, YANG J R, CHEN C Y, HONG W. Grain structure and co-precipitation behavior of high-Zn containing Al−Zn−Mg−Cu aluminium alloys during deformation via high- temperature upsetting-extrusion [J]. Journal of Alloys and Compounds, 2023, 968: 171871.

[7] DUCHAUSSOY A, DESCHAMPS A, SAUVAGE X, GEUSER F D, HORITA Z. Correlation between TEM, SAXS and DSC to investigate the influence of SPD on precipitation mechanisms of an Al−Zn−Mg−Cu alloy [J]. MATEC Web of Conferences, 2020, 326: 08006.

[8] HIDALGO-MANRIQUE P, OROZCO-CABALLERO A, CEPEDA-JIMÉNEZ C M, RUANO O A, CARREÑO F. Influence of the accumulative roll bonding process severity on the microstructure and superplastic behaviour of 7075 Al alloy [J]. Journal of Materials Science & Technology, 2016, 32(8): 774−782.

[9] YANG Yan-mei, LI Ye-fei, Yi Da-wei, ZHENG Qiao-ling, FANG Xue-wei, WANG Yong, CHANG Tian-xing, CHEN Ya-nan, GAO Yi-min, HUANG Ke. Revealing the microstructure evolution mechanism and mechanical responses of a novel Al−Zn−Mg−Cu alloy by hot deformation process [J]. Journal of Materials Research and Technology, 2024, 29: 3699−3710.

[10] ZHAO Jiu-hui, DENG Yun-lai, TANG Jian-guo, ZHANG Jin. Effect introduced high density of precipitates on the microstructural evolutions during multi-direction forging of Al−Zn−Mg−Cu alloy [J]. Materials Science and Engineering: A, 2020, 798: 139927.

[11] ZHANG W G, YE Y C, HE L J, LI P J, FENG X Q, NOVIKOV L S. Dynamic response and micro- structure control of Al-Sc binary alloy under high-speed impact [J]. Materials Science and Engineering: A, 2013, 578: 35−45.

[12] ZHOU Ying-hui, WANG Zhen-nan, LIN Xin, JIAN Zeng-yun, LIU Yong-qin, REN Yong-ming, ZHANG Tian-chi, SHAO Wen-ting, YANG Xi-gang. Impact toughness and fractography of diverse microstructure in Al−Cu alloy fabricated by arc-directed energy deposition [J]. Additive Manufacturing, 2023, 63: 103414.

[13] LU Jue, SONG Yan-li, ZHOU Pu, XU Hai-nan, LIU Yu-jian, HUA Lin. Effect of thermal strain on the microstructure evolution and post-aging mechanical properties of Al−Zn−Mg−Cu alloy in simulating hot stamping process [J]. Materials Science and Engineering: A, 2023, 880: 145316.

[14] FAN Cai-he, OU Ling, HU Ze-yi, YANG Jian-jun, CHEN Xi-hong. Re-dissolution and re-precipitation behavior of nano-precipitated phase in Al−Cu−Mg alloy subjected to rapid cold stamping [J].Transactions of Nonferrous Metals Society of China, 2019, 29(12): 2455−2462.

[15] SHEN Gao-liang, XIANG Zhi-lei, MA Zhi-lei, HUANG Jing-cun, ZHAO Yue-qing, LI Ji-hao, WANG Zhi-tian, SHI Guo-dong, CHEN Zi-yong. Investigation of microstructures and mechanical properties of ultra-high strength Al−Zn−Mg−Cu alloy prepared by rapid solidification and hot extrusion [J]. Metals, 2023, 13(2): 293.

[16] LI Gui-sheng, PAN Xin-yuan, JIANG Jin, LI Jing-hui, XIE Ling-ling, LIU Hai-tao, ZHANG Ming-ya. Achieving ultra-fine grains and high corrosion resistance of Al−Zn−Mg−Cu alloy by ECAP and post cold rolling [J]. Journal of Materials Research and Technology, 2023, 267: 354−7368.

[17] LI Yi-hui. Research on the influence of cold rolling deformation on the structure and properties of spray formed Al−Zn−Mg−Cu extruded alloy [D]. Xiangtan: Hunan University of Technology, 2023. (in Chinese)

[18] SUN Zhi-chao, ZHENG Li-shuang, YANG He. Softening mechanism and microstructure evolution of as-extruded 7075 aluminum alloy during hot deformation [J]. Materials Characterization, 2014, 90: 71−80.

[19] LIU Jing, YAO Pei, ZHAO Nai-qin, SHI Chun-sheng, LI Hui-jun, LI Xuan, XI De-sheng, YANG Shuo. Effect of minor Sc and Zr on recrystallization behavior and mechanical properties of novel Al−Zn−Mg−Cu alloys [J]. Journal of Alloys and Compounds, 2016, 657: 717−725.

[20] LIN Yong-cheng, ZHU Xu-Hao, DONG Wen-yong, YANG Hui, XIAO Yi-wei, KOTKUNDE N. Effects of deformation parameters and stress triaxiality on the fracture behaviors and microstructural evolution of an Al−Zn−Mg−Cu alloy [J]. Journal of Alloys and Compounds, 2020, 832: 154988.

[21] XIAO Wen-chao, WANG Bao-yu, WU Yong, YANG Xiao-ming. Constitutive modeling of flow behavior and microstructure evolution of AA7075 in hot tensile deformation [J]. Materials Science and Engineering: A, 2018, 712: 704−713.

[22] ZANG Qian-hao, YU Hua-shun, LEE Y S, KIM M S, KIM H W. Hot deformation behavior and microstructure evolution of annealed Al−7.9Zn−2.7Mg−2.0Cu (wt.%) alloy [J]. Journal of Alloys and Compounds, 2018, 763: 25−33.

[23] FAN Cai-he, LI Yi-hui, WU Qin, YANG Jian-jun, NI Yu-meng, DING Liu-xin. Effect of cold rolling deformation on the microstructure and mechanical properties of spray-formed Al−Zn−Mg−Cu alloy [J]. Journal of Materials Research, 2024, 39(3): 471−479.

[24] HUO W T, SHI J T, HOU L G, ZHANG J S. An improved thermo-mechanical treatment of high-strength Al−Zn−Mg−Cu alloy for effective grain refinement and ductility

modification [J]. Journal of Materials Processing Technology, 2017, 239: 303−314.
[25] ZUO Jin-rong, HOU Long-gang, SHU Xue-dao, PENG Wen-fei, YIN An-min, ZHANG Ji-shan. Grain refinement assisted by deformation enhanced precipitates through thermomechanical treatment of AA7055 Al alloy [J]. Metals, 2020, 10(5): 594.
[26] MEI L, YANG M J, CHEN X P, JIN Q Q, WANG Y Q, LI Y M. Precipitate evolution and properties of an Al−Zn−Mg−Cu alloy processed by thermomechanical treatment [J]. Materials Science and Engineering: A, 2023, 867: 144716.
[27] CHEN Zhi-guo, YUAN Zhen-gui, REN Jie-ke. The mechanism of comprehensive properties enhancement in Al−Zn−Mg−Cu alloy via novel thermomechanical treatment [J]. Journal of Alloys and Compounds, 2020, 828: 154446.
[28] WANG Yin, LI Yong, YU Wei, TANG Hong-qun, WANG Hai-yao, XU Guang-ming, WANG Zhao-dong. Effect of a special thermo-mechanical treatment process on microstructure and properties of 7185 alloy [J]. Journal of Alloys and Compounds, 2023, 935: 168072.
[29] WANG Chen, MA Li-nan, MA Xiao-guang, WANG Tao, JIANG Zheng-yi, HASAN M, ZHAO Jing-wei. Effect of annealing temperature on microstructure and tensile properties of copper/aluminum composite thin strip [J]. Transactions of Nonferrous Metals Society of China, 2023, 33(3): 701−713.
[30] KAZEMI-NAVAEE A, JAMAATI R, JAMSHIDI AVAL H. Effect of single roll drive rolling on microstructure, texture, and mechanical property anisotropy of Al−5.6Zn−2.5Mg−1.4Cu aluminum alloy [J]. Transactions of Nonferrous Metals Society of China, 2023, 33(11): 3266−3281.
[31] FAN Xiao-yu, LI Yu, XU Chun, WANG Bin-jun, PENG Rui-zhi, CHEN Jian-bin. Improved mechanical anisotropy and texture optimization of a 3xx aluminum alloy by differential temperature rolling [J]. Materials Science and Engineering: A, 2021, 799: 140278.
[32] HARRELL T J, TOPPING T D, WEN Hai-ming, HU Tao, SCHOENUNG J M, LAVERNIA E J. Microstructure and strengthening mechanisms in an ultrafine grained Al−Mg−Sc alloy produced by powder metallurgy [J]. Metallurgical and Materials Transactions A, 2014, 45: 6329−6343.
[33] MA Ka-ka, WEN Hai-ming, HU Tao, TOPPING T D, ISHEIM D, SEIDMAN D N, LAVERNI E J, SCHOENUNG J M. Mechanical behavior and strengthening mechanisms in ultrafine grain precipitation-strengthened aluminum alloy [J]. Acta Materialia, 2014, 62: 141−155.
[34] ZRIBI Z, KTARI H H, HERBST F, OPTASANU V, NJAH N. EBSD, XRD and SRS characterization of a casting Al−7wt.%Si alloy processed by equal channel angular extrusion: Dislocation density evaluation [J]. Materials Characterization, 2019, 153: 190−198.
[35] MA Ka-ka, HU Tao, YANG H, TOPPING T, YOUSEFIANI A, LAVERNIA E J, SCHOENUNG J M. Coupling of dislocations and precipitates: Impact on the mechanical behavior of ultrafine grained Al−Zn−Mg alloys [J]. Acta Materialia, 2016, 103: 153−164.
[36] ZHAO Wei, JIANG Zhi-hao, WU Xiang, LIU Yu-jing, YANG Hao-kun, WANG Jun, LIU Qi, LIU Xiao-chun. Anomalous $\{10\bar{1}2\}$ tensile twinning and subsequent detwinning in a friction stir processed carbon fiber-reinforced Mg composite [J]. Journal of Magnesium and Alloys, 2024, 12: 1511−15177.
[37] FAN Cai-he, LI Yi-hui, WU Qin, HU Ze-yi, NI Yu-meng, YANG Jian-jun. Effect of cold rolling deformation on microstructure evolution and mechanical properties of spray formed Al−Zn−Mg−Cu−Cr alloys [J]. Transactions of Nonferrous Metals Society of China, 2024, 34(8): 2442−2454.

快速冷冲对喷射成形 Al−Zn−Mg−Cu 合金显微组织和力学性能的影响

范才河，李 济，杨双君，胡泽艺，吴 琴，欧 玲，武 帅

湖南工业大学 材料科学与工程学院，株洲 412007

摘 要：采用 X 射线衍射(XRD)、扫描电子显微镜(SEM)、能量色散光谱(EDS)、电子背散射衍射(EBSD)和透射电子显微镜(TEM)，系统研究在常温条件下快速冷冲对喷射成形 Al−Zn−Mg−Cu 合金显微组织演变和力学性能的影响。结果表明，随着冷冲次数的增加，样品的位错密度升高，第二相($Mg(Zn,Cu,Al)_2$ 相)的体积分数从 15.64%增加至 23.94%，平均尺寸从 1.41 μm 减小至 0.75 μm。第二相对位错的钉扎作用促使低角度晶界向高角度晶界显著转变，导致平均晶粒尺寸从 5.75 μm 减小至 0.97 μm。随着冷冲次数的增加，样品的强度和硬度提高，这归因于位错强化、晶界强化和第二相强化的协同效应。

关键词：Al−Zn−Mg−Cu 合金；快速冷冲；织构；亚晶界；第二相

(Edited by Xiang-qun LI)